Robust Safety-Preserving Rendezvous Control for Coordinated Heterogeneous Marine Vehicles: An Observer-Based Structure-Keeping Port-Hamiltonian Approach

Zehua Jia, *Member, IEEE*, Huahuan Wang, *Student Member, IEEE*, Wentao Wu, *Member, IEEE*, Guoqing Zhang, *Member, IEEE*, and Weidong Zhang, *Senior Member, IEEE*

***Abstract*—This article studies the 3-D dynamic rendezvous control problem for coordinated heterogeneous marine vehicles, including an uncrewed underwater vehicle (UUV) and an autonomous surface vehicle (ASV). An observer-based safety-preserving rendezvous control approach is proposed to robustly stabilize the rendezvous errors under the port-Hamiltonian (PH) framework. First, an interconnection and damping assignment passivity-based control (IDA-PBC) method is adopted to provide a basic stabilizing control framework. In this problem, both vehicles are faced with hydrodynamic model uncertainties and unknown external disturbances. Then, to preserve the rendezvous safety under uncertain dynamics, the prescribed performance control (PPC) transformation is implemented for the ascending motion to get the equivalent approaching-constrained PH system. The intuitive design procedure provided by the IDA-PBC method, along with the collision-free rendezvous safety guaranteed by the auxiliary PPC technique, reduces the controller design complexity while providing a smooth rendezvous trajectory. Besides, a structure-keeping uncertainty observer algorithm is designed and incorporated to simultaneously handle model uncertainties and environmental disturbances without destroying the interconnection structure. Under the proposed approach, the UUV-ASV rendezvous errors can be effectively stabilized with rigorous closed-loop stability analysis. Finally, both simulations and comparative experiments are conducted to demonstrate the effectiveness and advantages of the proposed approach.**

***Index Terms*—Autonomous surface vehicle (ASV), coordinated control, port-Hamiltonian (PH) theory, uncertainty observer, uncrewed underwater vehicle (UUV).**

Received 17 September 2025; revised 4 December 2025; accepted 30 December 2025. This work was supported in part by the National Natural Science Foundation of China under Grant 52501388 and Grant U24A20260, in part by Hainan Provincial Natural Science Foundation of China under Grant 425RC697, and in part by Hainan Province Science and Technology Special Fund under Grant ZDYF2024GXJS003. This article was recommended by Associate Editor D. Dong. *(Corresponding author: Weidong Zhang.)*

Zehua Jia and Huahuan Wang are with the School of Information and Communication Engineering, Hainan University, Haikou 570228, China (e-mail: zhjia@hainanu.edu.cn; whh@hainanu.edu.cn).

Wentao Wu is with the School of Automation and Intelligent Sensing, Shanghai Jiao Tong University, Shanghai, 200240 China (e-mail: wentao-wu@sjtu.edu.cn).

Guoqing Zhang is with the Navigation College, Dalian Maritime University, Dalian 116026, China (e-mail: zgq_dlmu@163.com).

Weidong Zhang is with the School of Information and Communication Engineering, Hainan University, Haikou 570228, China, and also with the School of Automation and Intelligent Sensing, Shanghai Jiao Tong University, Shanghai 200240, China (e-mail: wdzhang@sjtu.edu.cn).

Color versions of one or more figures in this article are available at https://doi.org/10.1109/TCYB.2026.3652215.

Digital Object Identifier 10.1109/TCYB.2026.3652215

I. Introduction

With the rapid advancement of ocean exploration, autonomous marine vehicles (AMVs) capable of providing efficient and low-cost exploration services have gained a surge in marine applications. Over the last two decades, many researchers attempted to investigate various control strategies for single AMV control problems that involve dynamic positioning [1], [2], [3], [4], path following [5], [6], [7], [8], [9], and trajectory tracking [10], [11], [12], [13]. However, for tasks that require cross-domain cooperation and long-term offshore operations, such as offshore maritime search [14], maritime emergency disaster relief [15], and multidimensional ocean observations [16], AMVs usually need to execute tasks in a coordinated manner. A representative case is the coordinated surface-underwater search for Malaysia Airlines MH-370. Since different types of AMVs have distinct operational capabilities, the coordination of heterogeneous AMVs can significantly improve operational efficiency and expand the operating range.

Compared with homogeneous systems [17], [18], [19], some control strategies have been proposed recently for the coordination problems of heterogeneous systems. Except for some model-free control schemes that do not require explicit system dynamics [20], [21], [22], [23], existing model-based methods can be generally classified into the optimization-based approach and the nonoptimization approach. A typical optimization-based control method is model predictive control (MPC), which is widely applied in heterogeneous systems. In [24], a disturbance compensating model predictive control (DMPC) method was proposed. By sequentially solving optimal control and disturbance compensation problems, the designed controller can achieve robust cooperation for heterogeneous AMVs. In [25], the cooperation problem of autonomous aerial vehicles (AAVs) and autonomous ground vehicles (AGVs) in the presence of external disturbances and denial of service attacks was studied based on DMPC. In [14],

a safety-preserving Lyapunov-based MPC framework was presented to accomplish coordinated rendezvous of an uncrewed underwater vehicle (UUV) and an autonomous surface vehicle (ASV) subject to external disturbances. In [26], a distributed event-triggered adaptive MPC method was proposed for the formation control of the AAV-ASV. With the optimization-enabled capabilities, the above methods provide promising results for heterogeneous vehicles. However, practical model uncertainty problems cannot be handled due to the high dependence on accurate modeling.

Unlike the optimization-based control method, the nonoptimization-based method can directly handle model uncertainties and disturbances with various techniques in a computationally tractable way. For instance, in [27], a decentralized formation control scheme based on the sliding mode technique and extended state observers was presented for the heterogeneous UUV-ASV system under external disturbances and unmodeled dynamics. In [28] and [29], observer-based fault-tolerant fixed-time control methods were proposed for multiple AAVs formation under disturbances and uncertainties with and without the prescribed performance control (PPC) technique, respectively. Although the above methods achieve satisfactory control performance, intervehicle safety (e.g., collision avoidance) was not considered, especially when faced with unknown disturbances and model uncertainties. In addition to the intervehicle safety, the engineering applicability is another problem that needs to be considered. In practical engineering applications, algorithms with concise forms and clear interpretability are often preferred since they are more engineer-friendly. However, most of the advanced nonlinear control designs, for example, backstepping, sliding mode, and so on, are quite complicated and not intuitive, including the aforementioned methods [27], [28], [29]. One reason is that the design procedure of those methods is more like doing signal processing, which can be called "signal-based" methods and does not directly reflect the physical features of the system.

Different from "signal-based" methods, port-Hamiltonian (PH) theory provides a unified framework to describe and analyze physical–mechanical systems from the perspective of "energy flow" [30], [31]. By establishing the conceptual relationship between energy conservation and dissipation, the PH framework enables controller design with clear physical interpretations. Among its methodologies, one of the most representative is the interconnection and damping assignment passivity-based control (IDA-PBC) [32], which has become a cornerstone in PH-based control design. In recent years, PH-based methods have been applied to autonomous marine vehicles (AMVs). For example, in [33], PH theory was used for dynamic positioning of ships, while [34] developed a PH-based algorithm extending $\mathscr{L}_2$ disturbance attenuation for UUVs. More recently, a fixed-time tracking control strategy under external disturbances was proposed in [35] for UUVs. In addition to marine vehicles, PH-based control techniques have been extended to a wide spectrum of mechanical systems, such as robotic arms actuated by artificial muscles [36], autonomous ground vehicles [37], and advanced flight control systems [38]. Following the energy-shaping idea, pioneering works have combined IDA-PBC with integral actions to address unknown disturbances [39], [40], and an adaptive IDA-PBC approach was proposed in [41] to handle constant disturbances and unmodeled dynamics in UUV tracking. However, the controllers in [34], [35], [36], [37], [38], [39], [40], and [41] cannot simultaneously cope with time-varying disturbances and unmodeled dynamics, and most of them mainly focus on achieving motion behaviors without explicitly considering safety constraints. In contrast, when dealing with multiple AMVs' cooperation under uncertain dynamics, it is critical to account for both intervehicle safety and robustness against disturbances.

Motivated by the above discussions, this article aims to develop a safety-preserving coordinated rendezvous control approach for UUV-ASV systems to achieve the dynamic 3-D rendezvous in the presence of unknown disturbances and unmodeled dynamics. From an energy-flow perspective, an IDA-PBC-based rendezvous control scheme is proposed under the PH framework. Based on the PH structure, a novel structure-keeping uncertainty observer (SKUOB) technique is developed to simultaneously handle external disturbances and unmodeled dynamics. By further incorporating the PPC transformation into the IDA-PBC framework, the designed observer-based structure-keeping interconnection and damping assignment (OSK-IDA) method can directly preserve the intervehicle safety by achieving a collision-free rendezvous. The main contributions of this article are summarized as follows.

1) In contrast to the "signal-based" design methods [27], [29], which require tricky transformation or complicated calculations for intermediate system signals, the proposed IDA-PBC controller is derived by solving energy-reshaped matching equations, making the design more intuitive. The unique dissipation property of the PH system enhances the physical interpretation of the design procedure.
2) The integration of the PPC technique within the IDA-PBC framework serves as a key auxiliary design that facilitates the transformation of the original constrained control problem into an equivalent unconstrained problem. Unlike other IDA-PBC approaches [41], [42], which cannot handle potential intervehicle collision, the proposed OSK-IDA controller can ensure the rendezvous safety by utilizing the PPC-transformed state as the PH state.
3) Compared with the IDA-PBC methods in [43], [44], and [45], where the controllers cannot handle model uncertainties and the method in [41], where the controller can only address constant disturbances and model uncertainties within the PH framework, the proposed SKUOB-aided method can effectively handle time-varying disturbances and unmodeled dynamics simultaneously without destroying the intrinsic interconnection structure presented by the PH system.

II. Problem Formulation

In this section, the adopted models of the heterogeneous marine vehicles are introduced first, and then the control objective and preliminaries are briefly specified. For the sake

of subsequent expressions, the subscripts "u" and "a" represent the corresponding variables of the UUV and ASV, respectively.

A. UUV Modeling

According to the mathematical models presented in [46], the UUV model can be expressed as follows:

$$\begin{aligned}\dot{\boldsymbol{\eta}}_u &= \boldsymbol{J}_u\left(\boldsymbol{\eta}_u\right)\boldsymbol{\nu}_u\\ \boldsymbol{M}_u\dot{\boldsymbol{\nu}}_u &= -\boldsymbol{C}_u\boldsymbol{\nu}_u - \boldsymbol{D}_u\boldsymbol{\nu}_u - \boldsymbol{g}\left(\boldsymbol{\eta}_u\right) + \boldsymbol{\tau}_u + \boldsymbol{d}_u\end{aligned} \tag{1}$$

where $\boldsymbol{\eta}_u = [x_u, y_u, z_u, \phi_u, \theta_u, \psi_u]^\top$ represents the position vector in the inertial frame. $\boldsymbol{\nu}_u = [u_u, v_u, w_u, p_u, q_u, r_u]^\top$ represents the velocity vector in the body-fixed frame. ϕ_u, θ_u, and ψ_u are the rotational angles of the UUV in roll, pitch, and yaw directions. $\boldsymbol{J}_u = \text{diag}\{\boldsymbol{J}_{u1}, \boldsymbol{J}_{u2}\} \in \mathbb{R}^{6\times6}$ denotes the rotation matrix between the earth frame and the body-fixed frame. $\boldsymbol{D}_u = \text{diag}\{X_{|u|}|u_u| + X_u, Y_{|v|}|v_u| + Y_v, Z_{|w|}|w_u| + Z_w, K_{|p|}|p_u| + K_p, M_{|q|}|q_u| + M_q, N_{|r|}|r_u| + N_r\}$ is the symmetric damping matrix, composed of both linear and nonlinear damping components, where $X_{|u|}$, X_u, $Y_{|v|}$, Y_v, $Z_{|w|}$, Z_w, $K_{|p|}$, K_p, $M_{|q|}$, M_q, $N_{|r|}$, and N_r are the hydrodynamic coefficients. $\boldsymbol{\tau}_u \in \mathbb{R}^{6\times1}$ and $\boldsymbol{d}_u \in \mathbb{R}^{6\times1}$ are the force input and the unknown external disturbance, respectively. $\boldsymbol{g}(\boldsymbol{\eta}_u) = [(G-B)s\theta_u, -(G-B)s\phi_u c\theta_u, -(G-B)c\phi_u c\theta_u, y_b Bc\phi_u c\theta_u - z_b Bs\phi_u c\theta_u, -z_b Bs\theta_u - x_b Bc\phi_u c\theta_u, x_b Bs\phi_u c\theta_u + y_b Bs\theta_u]^\top$ is the resorting force, where signs $c(\cdot)$, $s(\cdot)$, and $t(\cdot)$ denote $\cos(\cdot)$, $\sin(\cdot)$, and $\tan(\cdot)$, respectively. $G = mg_0$ and $B = bg_0$ are the gravity and buoyancy of the UUV, respectively. b and g_0 are the buoyancy constant and the gravitational constant. x_b, y_b, and z_b are the position coordinates of the buoyant center relative to the center of gravity in the body-fixed system. The matrix $\boldsymbol{M}_u = \text{diag}\{m-X_{\dot{u}}, m-Y_{\dot{v}}, m-Z_{\dot{w}}, I_x-K_{\dot{p}}, I_y-M_{\dot{q}}, I_z-N_{\dot{r}}\} \in \mathbb{R}^{6\times6}$ is the inertia matrix, where m is the UUV mass. I_x, I_y, and I_z are the moments of inertia. $X_{\dot{u}}$, $Y_{\dot{v}}$, $Z_{\dot{w}}$, $K_{\dot{p}}$, $M_{\dot{q}}$, and $N_{\dot{r}}$ are added mass coefficients. $\boldsymbol{C}_u \in \mathbb{R}^{6\times6}$ is the Coriolis–centripetal matrix consisting of the rigid-body Coriolis matrix $\boldsymbol{C}_{RB}$ and the hydrodynamic added Coriolis matrix $\boldsymbol{C}_A$ with specific expressions given below:

$$\boldsymbol{C}_{RB} = \begin{bmatrix}\boldsymbol{0}_{3\times3} & -m\boldsymbol{\Omega}\left(\boldsymbol{\nu}_{\bar{T}}\right)\\ -m\boldsymbol{\Omega}\left(\boldsymbol{\nu}_{\bar{T}}\right) & -\boldsymbol{\Omega}\left(\boldsymbol{I}_0\boldsymbol{\nu}_R\right)\end{bmatrix}, \boldsymbol{C}_A = \begin{bmatrix}\boldsymbol{0}_{3\times3} & \boldsymbol{\Omega}\left(\boldsymbol{\zeta}_{\bar{T}}\right)\\ \boldsymbol{\Omega}\left(\boldsymbol{\zeta}_{\bar{T}}\right) & \boldsymbol{\Omega}\left(\boldsymbol{\zeta}_R\right)\end{bmatrix}$$

where $\boldsymbol{\nu}_{\bar{T}} = [u_u, v_u, w_u]^\top$ and $\boldsymbol{\nu}_R = [p_u, q_u, r_u]^\top$ denote the translational and rotational velocities, respectively. In the above definitions, $\boldsymbol{\zeta}_{\bar{T}} = [X_{\dot{u}}u_u, Y_{\dot{v}}v_u, Z_{\dot{w}}w_u]^\top$, $\boldsymbol{\zeta}_R = [K_{\dot{p}}p_u, M_{\dot{q}}q_u, N_{\dot{r}}r_u]^\top$, and $\boldsymbol{I}_0 = \text{diag}(I_x, I_y, I_z)$. The cross-product operator $\boldsymbol{\Omega}(\cdot)$ is defined as follows:

$$\boldsymbol{\Omega}\left(\bar{\boldsymbol{\nu}}\right) = \begin{bmatrix}0 & -\bar{\nu}(3) & \bar{\nu}(2)\\ \bar{\nu}(3) & 0 & -\bar{\nu}(1)\\ -\bar{\nu}(2) & \bar{\nu}(1) & 0\end{bmatrix}$$

where $\bar{\boldsymbol{\nu}} \in \mathbb{R}^{3\times1}$ can be any 3-D vector.

TABLE I
MODEL PARAMETERS

Name	Value	Name	Value	Name	Value
m_{11}	25.80	m_{22}	33.80	m_{33}	2.760
m	125	$X_{\dot{u}}$	-167.6	X_u	26.9
b	125	$Y_{\dot{v}}$	-477.2	Y_v	35.8
g_0	9.81	$Z_{\dot{w}}$	-383	Z_w	0
I_x	9.3	$K_{\dot{p}}$	-11.6	K_p	3.0
I_y	14.9	$M_{\dot{q}}$	-15.5	M_q	4.9
I_z	13.1	$N_{\dot{r}}$	-15.9	N_r	3.5
x_b	0	y_b	0	z_b	-0.04298
$X_{\|u\|u}$	241.3	$Y_{\|v\|v}$	503.8	$Z_{\|w\|w}$	265.6
$K_{\|p\|p}$	101.6	$M_{\|q\|q}$	59.9	$N_{\|r\|r}$	76.9
d_{11}	$2.5\|u_a\| + 12$	d_{22}	$4.5\|v_a\| + 17$	d_{33}	$0.1\|r_a\| + 0.5$

Remark 1: The considered UUV is neutrally buoyant. Therefore, it satisfies $x_b = y_b = 0$ and $G = B$. Furthermore, the resorting force vector $\boldsymbol{g}(\boldsymbol{\eta}_u)$ is equivalent to $\boldsymbol{J}^\top(\boldsymbol{\eta}_u)\nabla_{\boldsymbol{\eta}_u}H_{u0}$ referring to [46] and can be rewritten as $\boldsymbol{g}(\boldsymbol{\eta}_u) = [0, 0, 0, z_b Bs\phi_u c\theta_u, z_b Bs\theta_u, 0]^\top$.

B. ASV Modeling

Considering the classical 3-DOF ASV model as follows [46]:

$$\begin{aligned}\dot{\boldsymbol{\eta}}_a &= \boldsymbol{J}_a\left(\boldsymbol{\eta}_a\right)\boldsymbol{\nu}_a\\ \boldsymbol{M}_a\dot{\boldsymbol{\nu}}_a &= -\boldsymbol{C}_a\boldsymbol{\nu}_a - \boldsymbol{D}_a\boldsymbol{\nu}_a + \boldsymbol{\tau}_a + \boldsymbol{d}_a\end{aligned} \tag{3}$$

where $\boldsymbol{\eta}_a = [x_a, y_a, \psi_a]^\top$ and $\boldsymbol{\nu}_a = [u_a, v_a, r_a]^\top$ denote the position and the velocity vectors in the inertial and body-fixed frames, respectively. ψ_a is the yaw angle. $\boldsymbol{\tau}_a \in \mathbb{R}^{3\times1}$ and $\boldsymbol{d}_a \in \mathbb{R}^{3\times1}$ are the control input and unknown external disturbance, respectively. $\boldsymbol{J}_a$ is the rotation matrix with its internal elements as $\boldsymbol{J}_{a(1,1)} = c\psi_a, \boldsymbol{J}_{a(1,2)} = -s\psi_a, \boldsymbol{J}_{a(2,1)} = s\psi_a, \boldsymbol{J}_{a(2,2)} = c\psi_a$, and $\boldsymbol{J}_{a(3,3)} = 1$. In the above equations, $\boldsymbol{M}_a = \text{diag}\{m_{11}, m_{22}, m_{33}\}$ is the inertia matrix, where m_{11}, m_{22}, and m_{33} denote mass components in body-fixed frame. $\boldsymbol{C}_a \in \mathbb{R}^{3\times3}$ is the Coriolis–centripetal matrix with its nonzero elements as $\boldsymbol{C}_{a(1,3)} = -m_{22}v_a$, $\boldsymbol{C}_{a(2,3)} = m_{11}u_a$, $\boldsymbol{C}_{a(3,1)} = m_{22}v_a$, and $\boldsymbol{C}_{a(3,2)} = -m_{11}u_a$. The hydrodynamic damping matrix $\boldsymbol{D}_a = \text{diag}\{d_{11}, d_{22}, d_{33}\}$, where d_{11}, d_{22}, and d_{33} are the hydrodynamic parameters including the angular quadratic damping factor and the angular linear damping factor. All parameters mentioned above are listed in Table I.

To facilitate discussions, we make the following assumptions in this article.

Assumption 1 ([47], [48]): In practical scenarios, the unknown external disturbances $\boldsymbol{d}_u$ and $\boldsymbol{d}_a$ are time-varying. Suppose that there exist positive constants d_{umax} and d_{amax} such that $\|\boldsymbol{d}_u\|_\infty \le d_{umax}$ and $\|\boldsymbol{d}_a\|_\infty \le d_{amax}$. Besides, the first derivatives of $\boldsymbol{d}_u$ and $\boldsymbol{d}_a$ are bounded by $\|\dot{\boldsymbol{d}}_i\|_\infty \le \bar{d}_i, i \in= u, a$, where $\bar{d}_i$ are positive constants.

$$\boldsymbol{J}_{u1} = \begin{bmatrix}c\theta_u c\psi_u & -c\phi_u s\psi_u + s\phi_u s\theta_u c\psi_u & s\phi_u s\psi_u + c\phi_u s\theta_u c\psi_u\\ c\theta_u s\psi_u & c\phi_u c\psi_u + s\phi_u s\theta_u s\psi_u & -s\phi_u s\psi_u + c\phi_u s\theta_u s\psi_u\\ -s\theta_u & s\phi_u c\theta_u & c\phi_u c\theta_u\end{bmatrix}, \boldsymbol{J}_{u2} = \begin{bmatrix}1 & s\phi_u t\theta_u & c\phi_u t\theta_u\\ 0 & c\phi_u & -s\phi_u\\ 0 & \frac{s\phi_u}{c\theta_u} & \frac{c\phi_u}{c\theta_u}\end{bmatrix} \tag{2}$$

Remark 2: For marine environments, disturbances mainly arise from currents, waves, and winds. Currents are usually low-frequency [46], while the inertia, viscosity, and finite energy of the fluid limit the rate of change of wind and wave loads [49], [50]. Specifically, wind loads, determined by wind speed and a trigonometric function of the attack angle, are also typically low frequency, and wave effects are often modeled as second-order, input-to-state stable systems [51]. As standard models treat these forces as continuous with bounded variation rates, the above assumption is both physically and mathematically reasonable in marine control applications.

C. Port-Hamiltonian Theory

The PH theory enables describing physical systems in port-based network models with respect to energy flow, providing an insightful and intuitive analysis of mechanical-physical systems, especially for AMVs. According to [52], a system can be called a PH system if it satisfies the following form:

$$\begin{aligned} \dot{\boldsymbol{x}} &= [\boldsymbol{L}(\boldsymbol{x}) - \boldsymbol{F}(\boldsymbol{x})]\nabla H(\boldsymbol{x}) + \boldsymbol{T}(\boldsymbol{x})\boldsymbol{u} \\ \boldsymbol{y} &= \boldsymbol{T}^{\top}(\boldsymbol{x})\nabla H(\boldsymbol{x}) \end{aligned} \tag{4}$$

where $\boldsymbol{x}$ and $\boldsymbol{y}$ are the state vector and the output vector, respectively. The skew-symmetric interconnection matrix $\boldsymbol{L}$ and the symmetric damping matrix $\boldsymbol{F}$ represent the internal energy exchange and energy dissipation of the PH system, respectively. $\boldsymbol{T}$ is the input matrix. The Hamiltonian function $H(\boldsymbol{x})$ denotes the total stored energy of the system.

By following the PH theory, the original Euler–Lagrange UUV model (1) can be reshaped in the PH form as follows:

$$\begin{bmatrix} \dot{\boldsymbol{\eta}}_u \\ \dot{\boldsymbol{p}}_u \end{bmatrix} = \begin{bmatrix} \boldsymbol{0}_{6\times 6} & \boldsymbol{J}_u \\ -\boldsymbol{J}_u^{\top} & -\boldsymbol{C}_u - \boldsymbol{D}_u \end{bmatrix} \begin{bmatrix} \nabla_{\boldsymbol{\eta}_u} H_{u0} \\ \nabla_{\boldsymbol{p}_u} H_{u0} \end{bmatrix} + \begin{bmatrix} \boldsymbol{0} \\ \boldsymbol{I} \end{bmatrix} \boldsymbol{\tau}_u + \begin{bmatrix} \boldsymbol{0} \\ \boldsymbol{d}_u \end{bmatrix} \tag{5}$$

where $\boldsymbol{I} \in \mathbb{R}^{6\times 6}$ is the identity matrix and $\boldsymbol{p}_u = \boldsymbol{M}_u \boldsymbol{\nu}_u$ denotes the momentum vector of the UUV. H_{u0} is the Hamiltonian (energy) function, which has the form of

$$H_{u0} = \frac{1}{2}\boldsymbol{p}_u^{\top}\boldsymbol{M}_u^{-1}\boldsymbol{p}_u + V(\boldsymbol{\eta}_u) \tag{6}$$

where $V(\boldsymbol{\eta}_u) = Gs(\theta_u)x_b - Gc(\theta_u)y_b - Gc(\theta_u)c(\phi_u)z_b$. For the ASV, selecting the Hamiltonian function H_{a0} as the kinetic energy [53]

$$H_{a0} = \frac{1}{2}\boldsymbol{p}_a^{\top}\boldsymbol{M}_a^{-1}\boldsymbol{p}_a \tag{7}$$

then the original Euler–Lagrange ASV model (6) can be also reshaped in the PH form

$$\begin{bmatrix} \dot{\boldsymbol{\eta}}_a \\ \dot{\boldsymbol{p}}_a \end{bmatrix} = \begin{bmatrix} \boldsymbol{0}_{3\times 3} & \boldsymbol{J}_a \\ -\boldsymbol{J}_a^{\top} & -\boldsymbol{C}_a - \boldsymbol{D}_a \end{bmatrix} \begin{bmatrix} \nabla_{\boldsymbol{\eta}_a} H_{a0} \\ \nabla_{\boldsymbol{p}_a} H_{a0} \end{bmatrix} + \begin{bmatrix} \boldsymbol{0} \\ \boldsymbol{I} \end{bmatrix} \boldsymbol{\tau}_a + \begin{bmatrix} \boldsymbol{0} \\ \boldsymbol{d}_a \end{bmatrix} \tag{8}$$

where $\boldsymbol{p}_a = \boldsymbol{M}_a \boldsymbol{\nu}_a$ denotes the momentum vector of the ASV and $\boldsymbol{I} \in \mathbb{R}^{3\times 3}$ is the identity matrix.

D. Prescribed Performance Control

The PPC technique ensures that the controlled system can achieve the prescribed performance under the dynamic response. This technique is widely applied in scenarios requiring high precision. Here, a function can be called the prescribed performance function if it satisfies the definition [54]

$$\rho(t) = \left\{ (\rho, t) \,|\, \rho > 0, \dot{\rho} < 0, \lim_{t\to\infty} \rho > 0 \right\} : \mathbb{R}^{+} \to \mathbb{R}^{+}.$$

Selecting a prescribed performance function in the form of $\rho(t) = (\rho_0 - \rho_\infty)e^{-\beta_0 t} + \rho_\infty$, and it can be observed that the selected prescribed performance function is decreasing exponentially. ρ_0 and ρ_∞ are nonnegative parameters, representing the initial and steady-state values, respectively. β_0 is the minimum convergence rate. Besides, the initial conditions also need to be satisfied, that is, $\rho_0 > \rho_\infty, -\alpha\rho(0) < x(0) < \beta\rho(0)$, where α and β are the designed constants, which impose the performance bounds on the output of the variable x requiring to be confined.

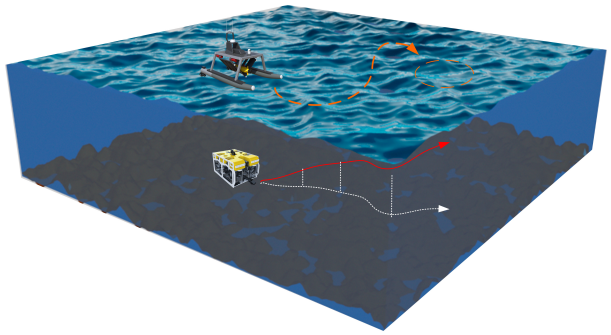

Fig. 1. Scenario illustration of the surface-underwater dynamic rendezvous.

E. Control Objective

Consider a practical scenario: after long-term oceanic exploration, a UUV in operation needs to be recharged while preserving its predefined mission as much as possible. To accomplish this task, an ASV is designated to autonomously follow the UUV and eventually rendezvous with it, serving as a mobile charging platform. During the dynamic rendezvous process, the ASV should gradually approach the moving UUV and then remain quasistationary relative to it, as illustrated in Fig. 1. For safety considerations, the rendezvous trajectory must be smooth and constrained to avoid potential collisions between the two vehicles. Accordingly, the control objective can be decomposed into the following components:

1) Rendezvous and Tracking Objectives: The UUV moves along a preset path. This tracking task can be expressed as $\| \tilde{\boldsymbol{\eta}}_u \|_{\infty} \leq c_1$, where $\tilde{\boldsymbol{\eta}}_u = \boldsymbol{\eta}_u - \boldsymbol{\eta}_{ud}$ is the tracking error vector of the UUV. $\boldsymbol{\eta}_{ud}$ denotes the desired trajectory position. c_1 is a small positive constant that bounds the tracking error. The ASV is required to follow the UUV. It can be described that the relative position error between the UUV and ASV in the horizontal plane needs to be converged over time, such that $\| \tilde{\boldsymbol{\eta}}_a \|_{\infty} \leq c_2$, where the ASV tracking error $\tilde{\boldsymbol{\eta}}_a$ is defined as $\tilde{\boldsymbol{\eta}}_a = \boldsymbol{\eta}_a - \boldsymbol{B}\boldsymbol{\eta}_u$, and $\boldsymbol{B} \in \mathbb{R}^{3\times 6}$ is the projection matrix with its nonzero elements as $\boldsymbol{B}_{(1,1)} = \boldsymbol{B}_{(2,2)} = \boldsymbol{B}_{(3,6)} = 1$. The threshold c_2 serves as an admissible upper bound on the rendezvous error $\tilde{\boldsymbol{\eta}}_a$ and can be selected based on the practical requirements of the rendezvous task. A smaller threshold corresponds to a more

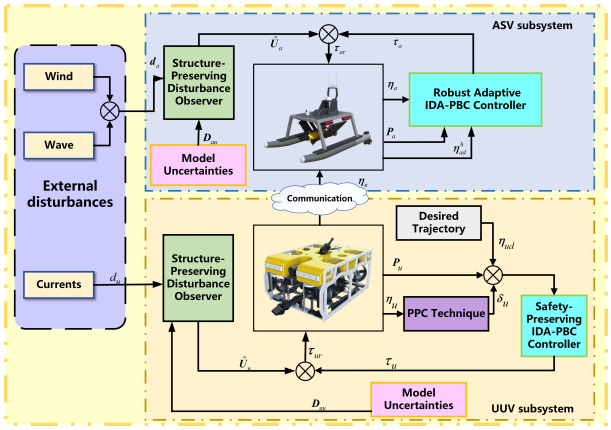

Fig. 2. Coordinated rendezvous control diagram of UUV-ASV systems.

stringent accuracy demand, whereas a larger value permits a more relaxed tolerance in rendezvous precision.

2) Ascending Objective: Since the investigated problem is a 3-D rendezvous, the UUV must gradually ascend to an admissible depth for subsequent docking. Therefore, the condition of the UUV is required as $z_u \to z_{ud}$, where z_{ud} denotes the admissible depth.

3) Safety Objective: Potential collision issues during the rendezvous between the UUV and ASV must be considered. The ascending depth of the UUV should not exceed the surface while maintaining a reasonable distance from it to enable the working of docking devices. Therefore, the UUV ascending motion should be confined and can be expressed as $z_u(t) > c_3, t \to \infty$, where c_3 is a preset constant greater than or equal to zero, representing the safety margin.

III. Controller Design

This section is divided into four parts. First, the safety-preserving rendezvous controllers for the UUV and ASV are designed using the IDA-PBC method assisted by the PPC technique. Second, a novel structure-keeping lumped uncertainty observer is developed to handle time-varying external disturbances and model uncertainties simultaneously. The rendezvous control scheme diagram is depicted in Fig. 2.

A. UUV Controller Design

With the consideration of rendezvous safety, we use the PPC technique to confine the UUV's ascending motion. To incorporate the PPC technique into the controller design, it is essential to transform the original heave state into an equivalent form [54]. The transformed equations are given as follows:

$$E_{z_u} = z_u(t) - z_{ud} = \rho(t) S(\varepsilon), S(\varepsilon) = \frac{\beta e^{\varepsilon} - \alpha e^{-\varepsilon}}{e^{\varepsilon} + e^{-\varepsilon}}$$

where E_{z_u} is the vertical rendezvous error of the UUV and ε is the equivalent state related to the vertical rendezvous error. $S(\varepsilon)$ possesses properties of smooth and monotonically decreasing. Through the inverse transformation of the above equations, ε is obtained as follows:

$$\varepsilon(t) = S^{-1}\left(\frac{E_{z_u}(t)}{\rho(t)}\right) = \frac{1}{2}\ln\frac{S+\alpha}{\beta - S}$$

from where we can see that if ε is bounded with the designed controller, the ascending error E_{z_u} can achieve the prescribed performance. In this article, the prescribed performance is set as a collision-free ascending trajectory. The derivative of ε can be calculated as follows:

$$\dot{\varepsilon} = \frac{1}{2\rho}\left(\frac{1}{S+\alpha} - \frac{1}{S-\beta}\right)\left(\dot{E}_{z_u} - \frac{E_{z_u}\dot{\rho}}{\rho}\right). \tag{9}$$

With the above state transformation between the variables ε and z_u, replacing $\dot{z}_u$ with $\dot{\varepsilon}$ in terms of the equivalent expression (9) into the original (1) yields

$$\dot{\boldsymbol{\delta}}_u = \bar{\boldsymbol{J}}_u \boldsymbol{\nu}_u + \boldsymbol{\Psi} \tag{10}$$

where $\boldsymbol{\Psi} = [0, 0, -\gamma S\dot{\rho}, 0, 0, 0]^{\top}$, and $\bar{\boldsymbol{J}}_u = \mathrm{diag}([1, 1, \gamma, 1, 1, 1])\boldsymbol{J}_u$. Here, $\gamma = 1/2\rho(1/(S+\alpha) - 1/(S-\beta))$. The new state $\boldsymbol{\delta}_u = [x_u, y_u, \varepsilon, \phi_u, \theta_u, \psi_u]^{\top}$ denotes the position vector of UUV rewritten based on the PPC technique, and it will be used in the IDA-PBC method. Following the design framework of the IDA-PBC method under the PH theory, the desired closed-loop PH structure can be constructed as follows:

$$\begin{bmatrix}\dot{\tilde{\boldsymbol{\delta}}}_u \\ \dot{\tilde{\boldsymbol{p}}}_u\end{bmatrix} = \begin{bmatrix}\boldsymbol{W}_{u11} & \boldsymbol{W}_{u12} \\ -\boldsymbol{W}_{u12}^{\top} & \boldsymbol{W}_{u22}\end{bmatrix}\nabla H_u \tag{11}$$

where $\tilde{\boldsymbol{\delta}}_u = \boldsymbol{\delta}_u - \boldsymbol{\delta}_{ud}$ and $\tilde{\boldsymbol{p}}_u = \boldsymbol{p}_u - \boldsymbol{p}_{ud}$ are position and momentum error vectors, respectively. Here, $\boldsymbol{\delta}_{ud}$ is the transformed desired trajectory with respect to $\boldsymbol{\eta}_{ud}$ and $\boldsymbol{p}_{ud}$ is the desired momentum which will be designed later. $\boldsymbol{W}_{u11}$ and $\boldsymbol{W}_{u22}$ are designed symmetric matrices, which are negative definite and symmetric. $\boldsymbol{W}_{u12}$ is an interconnection shaping matrix and needs to be designed later. H_u is the desired Hamiltonian function, and it can be designed as $H_u = 1/2\tilde{\boldsymbol{\delta}}_u^{\top}\boldsymbol{Q}_u\tilde{\boldsymbol{\delta}}_u + 1/2\tilde{\boldsymbol{p}}_u^{\top}\boldsymbol{R}_u^{-1}\tilde{\boldsymbol{p}}_u$, where $\boldsymbol{Q}_u$ and $\boldsymbol{R}_u$ are positive definite energy shaping matrices. By taking the derivative of $\tilde{\boldsymbol{\delta}}_u$ and substituting (10), one can get

$$\dot{\tilde{\boldsymbol{\delta}}}_u = \dot{\boldsymbol{\delta}}_u - \dot{\boldsymbol{\delta}}_{ud} = \bar{\boldsymbol{J}}_u\boldsymbol{\nu}_u + \boldsymbol{\Psi} - \dot{\boldsymbol{\delta}}_{ud}. \tag{12}$$

To reshape the system with the desired structure, the kinematic matching condition needs to be met first, that is, (12) needs to be matched to the first row of (11) as follows:

$$\dot{\tilde{\boldsymbol{\delta}}}_u = \bar{\boldsymbol{J}}_u\boldsymbol{\nu}_u + \boldsymbol{\Psi} - \dot{\boldsymbol{\delta}}_{ud} = \boldsymbol{W}_{u11}\boldsymbol{Q}_u\tilde{\boldsymbol{\delta}}_u + \boldsymbol{W}_{u12}\boldsymbol{R}_u^{-1}\tilde{\boldsymbol{p}}_u. \tag{13}$$

Since $\boldsymbol{\nu}_u = \boldsymbol{M}_u^{-1}\boldsymbol{p}_u$, to preserve the interconnection property of the PH system, $\boldsymbol{W}_{u12}$ is designed as follows:

$$\boldsymbol{W}_{u12} = \bar{\boldsymbol{J}}_u\boldsymbol{M}_u\boldsymbol{R}_u. \tag{14}$$

Then, the desired momentum vector is designed as follows:

$$\boldsymbol{p}_{ud} = \boldsymbol{M}_u\bar{\boldsymbol{J}}_u^{-1}\left(\boldsymbol{W}_{u11}\boldsymbol{Q}_u\tilde{\boldsymbol{\delta}}_u - \boldsymbol{\Psi} + \dot{\boldsymbol{\delta}}_{ud}\right). \tag{15}$$

Next, the kinetic matching condition needs to be met in a similar way to the kinematics. Taking the derivative of the momentum error vector, one can get

$$\dot{\tilde{\boldsymbol{p}}}_u = \dot{\boldsymbol{p}}_u - \dot{\boldsymbol{p}}_{ud}. \tag{16}$$

Substituting (1) into (16), and matching it to the second row of (11), one can get

$$-\boldsymbol{C}_u\boldsymbol{\nu}_u - \boldsymbol{D}_u\boldsymbol{\nu}_u - \boldsymbol{g} + \boldsymbol{\tau}_u + \boldsymbol{d}_u - \dot{\boldsymbol{p}}_{ud}$$

$$= -\boldsymbol{W}_{u12}^{\top}\boldsymbol{Q}_u\tilde{\boldsymbol{\delta}}_u + \boldsymbol{W}_{u22}\boldsymbol{R}_u^{-1}\tilde{\boldsymbol{p}}_u. \tag{17}$$

To get the basic IDA-PBC control laws, we first assume that there is no external disturbance in this part. Then, the following UUV tracking control law can be obtained by solving the matching equation:

$$\begin{aligned}\boldsymbol{\tau}_u = &-\boldsymbol{W}_{u12}^{\top}\boldsymbol{Q}_u\tilde{\boldsymbol{\delta}}_u + \boldsymbol{W}_{u22}\boldsymbol{R}_u^{-1}\tilde{\boldsymbol{p}}_u + \dot{\boldsymbol{p}}_{ud} \\ &+ \boldsymbol{C}_u\boldsymbol{\nu}_u + \boldsymbol{D}_u\boldsymbol{\nu}_u + \boldsymbol{g}.\end{aligned} \tag{18}$$

B. ASV Controller Design

The design procedure for the ASV is similar to the UUV. First, the desired closed-loop PH structure of the ASV is constructed as follows:

$$\begin{bmatrix}\dot{\tilde{\boldsymbol{\eta}}}_a \\ \dot{\tilde{\boldsymbol{p}}}_a\end{bmatrix} = \begin{bmatrix}\boldsymbol{W}_{a11} & \boldsymbol{W}_{a12} \\ -\boldsymbol{W}_{a12}^{\top} & \boldsymbol{W}_{a22}\end{bmatrix}\nabla H_a \tag{19}$$

where $\boldsymbol{W}_{a11}$ and $\boldsymbol{W}_{a22}$ are designed negative definite and symmetric matrices. The interconnection shaping matrix $\boldsymbol{W}_{a12}$ will be defined later. ∇H_a includes the partial derivatives of both the position and momentum of the ASV. H_a is the desired Hamiltonian function, and it is designed as $H_a = 1/2\tilde{\boldsymbol{\eta}}_a^{\top}\boldsymbol{Q}_a\tilde{\boldsymbol{\eta}}_a + 1/2\tilde{\boldsymbol{p}}_a^{\top}\boldsymbol{R}_a^{-1}\tilde{\boldsymbol{p}}_a$, where $\boldsymbol{Q}_a$ and $\boldsymbol{R}_a$ are positive definite energy shaping matrices.

For the kinematics of the ASV, its derivative in the form of error terms can be written as follows:

$$\dot{\tilde{\boldsymbol{\eta}}}_a = \dot{\boldsymbol{\eta}}_a - \boldsymbol{B}\boldsymbol{J}_u\boldsymbol{\nu}_u = \boldsymbol{J}_a\boldsymbol{\nu}_a - \boldsymbol{B}\boldsymbol{J}_u\boldsymbol{\nu}_u. \tag{20}$$

To reshape the system with the desired structure, the kinematic matching equation is supposed to hold, that is,

$$\dot{\tilde{\boldsymbol{\eta}}}_a = \boldsymbol{J}_a\boldsymbol{\nu}_a - \boldsymbol{B}\boldsymbol{J}_u\boldsymbol{\nu}_u = \boldsymbol{W}_{a11}\boldsymbol{Q}_a\tilde{\boldsymbol{\eta}}_a + \boldsymbol{W}_{a12}\boldsymbol{R}_a^{-1}\tilde{\boldsymbol{p}}_a \tag{21}$$

where the matrix $\boldsymbol{W}_{a12}$ is designed as follows:

$$\boldsymbol{W}_{a12} = \boldsymbol{J}_a\boldsymbol{M}_a\boldsymbol{R}_a. \tag{22}$$

Since $\boldsymbol{\nu}_a = \boldsymbol{M}_a^{-1}\boldsymbol{p}_a$, the desired virtual momentum vector $\boldsymbol{p}_{ad}$ can be designed as follows:

$$\boldsymbol{p}_{ad} = \boldsymbol{M}_a\boldsymbol{J}_a^{-1}\left(\boldsymbol{W}_{a11}\boldsymbol{Q}_a\tilde{\boldsymbol{\eta}}_a + \boldsymbol{B}\boldsymbol{J}_u\boldsymbol{\nu}_u\right). \tag{23}$$

For the kinetics of the ASV, taking the derivative of error vectors and matching it with the desired PH structure (19), one can get the following matching equation:

$$\dot{\tilde{\boldsymbol{p}}}_a = \dot{\boldsymbol{p}}_a - \dot{\boldsymbol{p}}_{ad} = -\boldsymbol{W}_{a12}^{\top}\boldsymbol{Q}_a\tilde{\boldsymbol{\eta}}_a + \boldsymbol{W}_{a22}\boldsymbol{R}_a^{-1}\tilde{\boldsymbol{p}}_a. \tag{24}$$

By substituting the original dynamic equations into the matching equation, the following control law can be obtained by solving the matching equation:

$$\begin{aligned}\boldsymbol{\tau}_a = &-\boldsymbol{W}_{a12}^{\top}\boldsymbol{Q}_a\tilde{\boldsymbol{\eta}}_a + \boldsymbol{W}_{a22}\boldsymbol{R}_a^{-1}\tilde{\boldsymbol{p}}_a + \dot{\boldsymbol{p}}_{ad} \\ &+ \boldsymbol{C}_a\boldsymbol{\nu}_a + \boldsymbol{D}_a\boldsymbol{\nu}_a.\end{aligned} \tag{25}$$

C. Observer-Based Structure-Keeping Control Design

In previous controller designs, all the control laws were designed without considering unmodeled dynamics or external disturbances. In practice, environmental disturbances widely exist and can hardly be measured. For marine vehicles, involved disturbances such as winds, waves, and ocean currents usually exhibit time-varying and low-frequency characteristics and directly affect vehicle maneuvering. In addition to environmental disturbances, model uncertainty is another factor that directly affects control performance. Since UUV and ASV models exhibit high nonlinearities and system identifications can be inaccurate, model uncertainties are inevitable in marine vehicle modeling and may lead to severe control deterioration. Therefore, it is necessary to handle model uncertainties and time-varying external disturbances simultaneously to improve the system's robustness. In this section, an interconnection structure-keeping uncertainty observing method is developed to estimate disturbances and model uncertainties simultaneously under the PH framework.

In practical engineering, due to the limited modeling accuracy, model uncertainties mainly stem from inaccurate hydrodynamic parameters. Since a group of inaccurate nominal parameters can be easily obtained by conducting basic experiments, the hydrodynamic damping matrix $\boldsymbol{D}_i$, $i \in \mathcal{N}$, can be decomposed into two parts

$$\boldsymbol{D}_i = \boldsymbol{D}_{i0} + \boldsymbol{D}_{iu} \tag{26}$$

where $\mathcal{N} = \{i | i = u, a\}$ is the vehicle node set. $\boldsymbol{D}_{i0}$ and $\boldsymbol{D}_{iu}$ are nominal and unmodeled parts, respectively. With this decomposition, the dynamic equations of the UUV and the ASV can be rewritten as follows:

$$\boldsymbol{M}_u\dot{\boldsymbol{\nu}}_u = -\left(\boldsymbol{C}_u + \boldsymbol{D}_{u0}\right)\boldsymbol{\nu}_u - \boldsymbol{g}_u + \boldsymbol{\tau}_u + \boldsymbol{d}_u - \boldsymbol{D}_{uu}\boldsymbol{\nu}_u \tag{27}$$

$$\boldsymbol{M}_a\dot{\boldsymbol{\nu}}_a = -\left(\boldsymbol{C}_a + \boldsymbol{D}_{a0}\right)\boldsymbol{\nu}_a + \boldsymbol{\tau}_a + \boldsymbol{d}_a - \boldsymbol{D}_{au}\boldsymbol{\nu}_a. \tag{28}$$

To consider all kinds of uncertainties, define the lumped uncertainties as $\boldsymbol{U}_i = \boldsymbol{d}_i - \boldsymbol{D}_{iu}\boldsymbol{\nu}_i$. Then, an intermediate variable $\boldsymbol{\alpha}_i$ is defined as follows:

$$\boldsymbol{\alpha}_i = \boldsymbol{U}_i - \boldsymbol{K}_i\boldsymbol{M}_i\boldsymbol{\nu}_i \tag{29}$$

where $\boldsymbol{K}_i$ is a positive-definite gain matrix. Take the time derivative of $\boldsymbol{\alpha}_i$, one can get

$$\begin{aligned}\dot{\boldsymbol{\alpha}}_u &= \dot{\boldsymbol{U}}_u - \boldsymbol{K}_u\boldsymbol{M}_u\dot{\boldsymbol{\nu}}_u \\ &= \dot{\boldsymbol{U}}_u - \boldsymbol{K}_u\left(-\left(\boldsymbol{C}_u + \boldsymbol{D}_{u0}\right)\boldsymbol{\nu}_u - \boldsymbol{g}_u + \boldsymbol{\tau}_u + \boldsymbol{U}_u\right) \\ \dot{\boldsymbol{\alpha}}_a &= \dot{\boldsymbol{U}}_a - \boldsymbol{K}_a\boldsymbol{M}_a\dot{\boldsymbol{\nu}}_a \\ &= \dot{\boldsymbol{U}}_a - \boldsymbol{K}_a\left(-\left(\boldsymbol{C}_a + \boldsymbol{D}_{a0}\right)\boldsymbol{\nu}_a + \boldsymbol{\tau}_a + \boldsymbol{U}_a\right).\end{aligned}$$

To proceed with the observer design, we first design the estimation laws for the intermediate variable $\boldsymbol{\alpha}_i$ as follows:

$$\dot{\hat{\boldsymbol{\alpha}}}_u = -\boldsymbol{K}_u\left\{-\left(\boldsymbol{C}_u + \boldsymbol{D}_{u0}\right)\boldsymbol{\nu}_u - \boldsymbol{g}_u + \boldsymbol{\tau}_u + \hat{\boldsymbol{U}}_u - \boldsymbol{K}_u^{-1}\boldsymbol{R}_u^{-1}\tilde{\boldsymbol{p}}_u\right\} \tag{30}$$

$$\dot{\hat{\boldsymbol{\alpha}}}_a = -\boldsymbol{K}_a\left\{-\left(\boldsymbol{C}_a + \boldsymbol{D}_{a0}\right)\boldsymbol{\nu}_a + \boldsymbol{\tau}_a + \hat{\boldsymbol{U}}_a - \boldsymbol{K}_a^{-1}\boldsymbol{R}_a^{-1}\tilde{\boldsymbol{p}}_a\right\} \tag{31}$$

then the lumped uncertainty observer is designed as follows:

$$\hat{\boldsymbol{U}}_i = \hat{\boldsymbol{\alpha}}_i + \boldsymbol{K}_i\boldsymbol{M}_i\boldsymbol{\nu}_i. \tag{32}$$

With the designed observer, we can design the observer-aided robust control laws based on the IDA-PBC controllers (18) and (25) designed in Section III-B as follows:

$$\begin{aligned}\boldsymbol{\tau}_{ur} &= -\boldsymbol{W}_{u12}^{\top}\boldsymbol{Q}_u\tilde{\boldsymbol{\delta}}_u + \boldsymbol{W}_{u22}\boldsymbol{R}_u^{-1}\tilde{\boldsymbol{p}}_u + \dot{\boldsymbol{p}}_{ud} \\ &\quad + \boldsymbol{C}_u\boldsymbol{\nu}_u + \boldsymbol{D}_{u0}\boldsymbol{\nu}_u + \boldsymbol{g}(\boldsymbol{\delta}_u) - \hat{\boldsymbol{U}}_u \qquad (33)\\ \boldsymbol{\tau}_{ar} &= -\boldsymbol{W}_{a12}^{\top}\boldsymbol{Q}_a\tilde{\boldsymbol{\eta}}_a + \boldsymbol{W}_{a22}\boldsymbol{R}_a^{-1}\tilde{\boldsymbol{p}}_a + \dot{\boldsymbol{p}}_{ad} \\ &\quad + \boldsymbol{C}_a\boldsymbol{\nu}_a + \boldsymbol{D}_{a0}\boldsymbol{\nu}_a - \hat{\boldsymbol{U}}_u. \qquad (34)\end{aligned}$$

It should be noted that the designed robust control laws can ensure the closed-loop system keeps the desired interconnection structure. This can be seen by taking the derivative of observation $\hat{\boldsymbol{U}}_i$

$$\dot{\hat{\boldsymbol{U}}}_i = \dot{\hat{\boldsymbol{\alpha}}}_i + \boldsymbol{K}_i\boldsymbol{M}_i\dot{\boldsymbol{\nu}}_i. \qquad (35)$$

By substituting (30) and (31) into (32), one can get the following result:

$$\hat{\boldsymbol{U}}_i = \boldsymbol{K}_i\tilde{\boldsymbol{U}}_i + \boldsymbol{R}_i^{-1}\tilde{\boldsymbol{p}}_i \qquad (36)$$

where $\tilde{\boldsymbol{U}}_i = \boldsymbol{U}_i - \hat{\boldsymbol{U}}_i$ is the observation error. Here, the derivative of observation not only contains the observation error, but also involves the momentum error, making the closed-loop an interconnection structure. To facilitate the following discussion, we define the Lyapunov candidate function for observers as $V_{oi} = \tilde{\boldsymbol{U}}_i^{\top}\boldsymbol{K}_{di}\tilde{\boldsymbol{U}}_i, \quad i \in \mathcal{N}$, where $\boldsymbol{K}_{di}$ is the gain matrix. More details of the observer-based controller analysis will be given in Section IV.

IV. Main Results

In this section, the overall closed-loop system stability is comprehensively analyzed.

Theorem 1: Suppose Assumption 1 holds. For heterogeneous marine vehicles (1) and (3) with Hamiltonian functions as (6) and (7), if the desired momentum are designed as (15) and (23), interconnection shaping matrices $\boldsymbol{W}_{u12}$ and $\boldsymbol{W}_{a12}$ are selected as (14) and (22), damping shaping matrices $\boldsymbol{W}_{u11}$, $\boldsymbol{W}_{u22}$, $\boldsymbol{W}_{a11}$, and $\boldsymbol{W}_{a22}$ are selected symmetric and negative definite, and gain matrices $\boldsymbol{Q}_i$, $\boldsymbol{R}_i$, $\boldsymbol{K}_i$, and $\boldsymbol{K}_{di}$, $i \in \mathcal{N}$, are selected symmetric and positive definite, coefficients σ_u and σ_a are selected appropriately such that $V_u(0) - b_u/\bar{c}_u > 0$, $\sigma_u\lambda_{\max}(\boldsymbol{K}_{du}) - \lambda_{\min}(\boldsymbol{K}_u) < 0$, $V_a(0) - b_a/\bar{c}_a > 0$, and $\sigma_a\lambda_{\max}(\boldsymbol{K}_{da}) - \lambda_{\min}(\boldsymbol{K}_a) < 0$, then the overall closed-loop UUV-ASV rendezvous system is input-to-state stable (ISS) and the collision-free rendezvous is guaranteed under the designed OSK-IDA control laws (33) and (34).

Proof: According to the PH theory and the reshaping measures designed in Section III, the closed-loop systems of the UUV and ASV can be expressed as the following PH forms along the designed control laws (33) and (34)

$$\begin{aligned}\begin{bmatrix}\dot{\tilde{\boldsymbol{\delta}}}_u\\ \dot{\tilde{\boldsymbol{p}}}_u\end{bmatrix} &= \begin{bmatrix}\boldsymbol{W}_{u11} & \boldsymbol{W}_{u12}\\ -\boldsymbol{W}_{u12}^{\top} & \boldsymbol{W}_{u22}\end{bmatrix}\nabla H_u + \begin{bmatrix}\boldsymbol{0}\\ \tilde{\boldsymbol{U}}_u\end{bmatrix}\\ \begin{bmatrix}\dot{\tilde{\boldsymbol{\eta}}}_a\\ \dot{\tilde{\boldsymbol{p}}}_a\end{bmatrix} &= \begin{bmatrix}\boldsymbol{W}_{a11} & \boldsymbol{W}_{a12}\\ -\boldsymbol{W}_{a12}^{\top} & \boldsymbol{W}_{a22}\end{bmatrix}\nabla H_a + \begin{bmatrix}\boldsymbol{0}\\ \tilde{\boldsymbol{U}}_a\end{bmatrix}. \qquad (37)\end{aligned}$$

In (37), the Hamiltonian functions H_u and H_a are original energy without uncertainties. To analyze the overall stability with considerations of lumped uncertainties, we define the total Hamiltonian function as follows:

$$H_{id} = H_i + \frac{1}{2}\tilde{\boldsymbol{U}}_i^{\top}\boldsymbol{K}_{di}\tilde{\boldsymbol{U}}_i, \quad i \in \mathcal{N} \qquad (38)$$

where H_{id} is the reshaped (desired) Hamiltonian function for the perturbed marine vehicle and $\tilde{\boldsymbol{U}}_i^{\top}\boldsymbol{K}_{di}\tilde{\boldsymbol{U}}_i$ represents the potential energy induced by observers. With the incorporated observers, define the augmented system states as $\boldsymbol{X}_u = [\tilde{\boldsymbol{\delta}}_u, \tilde{\boldsymbol{p}}_u, \tilde{\boldsymbol{U}}_u]^{\top}$ and $\boldsymbol{X}_a = [\tilde{\boldsymbol{\eta}}_a, \tilde{\boldsymbol{p}}_a, \tilde{\boldsymbol{U}}_a]^{\top}$. By using the dissipation property, the augmented closed-loop PH systems can thus be obtained as follows:

$$\begin{aligned}\begin{bmatrix}\dot{\tilde{\boldsymbol{\delta}}}_u\\ \dot{\tilde{\boldsymbol{p}}}_u\\ \dot{\tilde{\boldsymbol{U}}}_u\end{bmatrix} &= \begin{bmatrix}\boldsymbol{W}_{u11} & \boldsymbol{W}_{u12} & \boldsymbol{0}\\ -\boldsymbol{W}_{u12}^{\top} & \boldsymbol{W}_{u22} & \boldsymbol{I}\\ \boldsymbol{0} & -\boldsymbol{I} & -\boldsymbol{K}_u\boldsymbol{K}_{du}^{-1}\end{bmatrix}\nabla H_{ud} + \begin{bmatrix}\boldsymbol{0}\\ \boldsymbol{0}\\ \dot{\boldsymbol{U}}_u\end{bmatrix}\\ &= (\boldsymbol{L}_u - \boldsymbol{F}_u)\nabla H_{ud} + \boldsymbol{s}_u\\ \begin{bmatrix}\dot{\tilde{\boldsymbol{\eta}}}_a\\ \dot{\tilde{\boldsymbol{p}}}_a\\ \dot{\tilde{\boldsymbol{U}}}_a\end{bmatrix} &= \begin{bmatrix}\boldsymbol{W}_{a11} & \boldsymbol{W}_{a12} & \boldsymbol{0}\\ -\boldsymbol{W}_{a12}^{\top} & \boldsymbol{W}_{a22} & \boldsymbol{I}\\ \boldsymbol{0} & -\boldsymbol{I} & -\boldsymbol{K}_a\boldsymbol{K}_{da}^{-1}\end{bmatrix}\nabla H_{ad} + \begin{bmatrix}\boldsymbol{0}\\ \boldsymbol{0}\\ \dot{\boldsymbol{U}}_a\end{bmatrix}\\ &= (\boldsymbol{L}_a - \boldsymbol{F}_a)\nabla H_{ad} + \boldsymbol{s}_a \qquad (39)\end{aligned}$$

where $\boldsymbol{L}_i$ and $\boldsymbol{F}_i$ are reshaped interconnection and damping matrices that preserve the interconnection and dissipation structure. $\boldsymbol{s}_i$ represents the remaining right-hand side term.

For the closed-loop UUV and ASV systems, select the Hamiltonian function H_{id} as the Lyapunov candidate function, that is, $V_i = H_{id}$. Then, the overall Lyapunov candidate function for the UUV-ASV rendezvous system can be expressed as follows:

$$V = \sum_{i\in\mathcal{N}} V_i \qquad (40)$$

where V_i is the Lyapunov function of each subsystem, that is, UUV or ASV.

Take the stability analysis of the UUV as an example. Taking the derivative of V_u and substituting (39), one can get the following result:

$$\frac{dV_u}{dt} = \frac{\partial^{\top}H_{ud}}{\partial\boldsymbol{X}_u}\frac{d\boldsymbol{X}_u}{dt} = \frac{\partial^{\top}H_{ud}}{\partial\boldsymbol{X}_u}\left\{(\boldsymbol{L}_u - \boldsymbol{F}_u)\frac{\partial H_{ud}}{\partial\boldsymbol{X}_u} + \boldsymbol{s}_u\right\}.$$

Since the interconnection matrix $\boldsymbol{L}_u$ is skew-symmetric and the damping matrix $\boldsymbol{F}_u$ is symmetric and positive definite, the dissipation property is preserved, and the above equation can be further simplified as follows:

$$\begin{aligned}\frac{\mathrm{d}V_u}{\mathrm{d}t} &= \tilde{\boldsymbol{\delta}}_u^{\top}\boldsymbol{Q}_u\boldsymbol{W}_{u11}\boldsymbol{Q}_u\tilde{\boldsymbol{\delta}}_u + \tilde{\boldsymbol{p}}_u^{\top}\boldsymbol{R}_u^{-1}\boldsymbol{W}_{u22}\boldsymbol{R}_u^{-1}\tilde{\boldsymbol{p}}_u\\ &\quad + \tilde{\boldsymbol{U}}_u^{\top}\boldsymbol{K}_{du}\dot{\boldsymbol{U}}_u - \tilde{\boldsymbol{U}}_u^{\top}\boldsymbol{K}_{du}\boldsymbol{K}_u\tilde{\boldsymbol{U}}_u\\ &\le \tilde{\boldsymbol{\delta}}_u^{\top}\boldsymbol{Q}_u\boldsymbol{W}_{u11}\boldsymbol{Q}_u\tilde{\boldsymbol{\delta}}_u + \tilde{\boldsymbol{p}}_u^{\top}\boldsymbol{R}_u^{-1}\boldsymbol{W}_{u22}\boldsymbol{R}_u^{-1}\tilde{\boldsymbol{p}}_u\\ &\quad - \tilde{\boldsymbol{U}}_u^{\top}\boldsymbol{K}_{du}\boldsymbol{K}_u\tilde{\boldsymbol{U}}_u + \sigma_u\tilde{\boldsymbol{U}}_u^{\top}\boldsymbol{K}_{du}\boldsymbol{K}_{du}\tilde{\boldsymbol{U}}_u\\ &\quad + \frac{1}{4\sigma_u}\dot{\boldsymbol{U}}_u^{\top}\dot{\boldsymbol{U}}_u.\end{aligned}$$

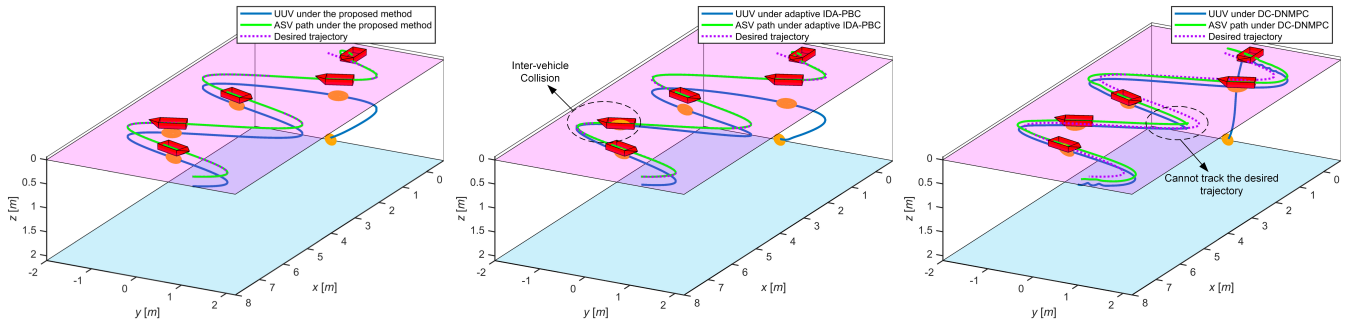

(a) (b) (c)

Fig. 3. Coordinated dynamic rendezvous trajectories under different methods. (a) Rendezvous results under the proposed method. (b) Rendezvous results under the method in [41]. (c) Rendezvous results under the method in [24].

Based on the properties of the generalized Rayleigh quotient, the aforementioned inequality is simplified as follows:

$$\begin{aligned}\frac{\mathrm{d}V_u}{\mathrm{d}t} &\le \lambda_{\max}\left(\boldsymbol{W}_{u11}\boldsymbol{Q}_u\right)\tilde{\boldsymbol{\delta}}_u^{\top}\boldsymbol{Q}_u\tilde{\boldsymbol{\delta}}_u + \frac{1}{4\sigma_u}\dot{\boldsymbol{U}}_u^{\top}\dot{\boldsymbol{U}}_u \\ &\quad + \left(\sigma_u\lambda_{\max}\left(\boldsymbol{K}_{du}\right) - \lambda_{\min}\left(\boldsymbol{K}_u\right)\right)\tilde{\boldsymbol{U}}_u^{\top}\boldsymbol{K}_{du}\tilde{\boldsymbol{U}}_u \\ &\quad + \lambda_{\max}\left(\boldsymbol{W}_{u22}\boldsymbol{R}_u^{-1}\right)\tilde{\boldsymbol{p}}_u^{\top}\boldsymbol{R}_u^{-1}\tilde{\boldsymbol{p}}_u \\ &\le -\bar{c}_u V_u + b_u.\end{aligned}$$

By further integrating the inequality over the interval $[0, t]$, one can obtain

$$0 \le V_u(t) \le \frac{b_u}{\bar{c}_u} + \left(V_u(0) - \frac{b_u}{\bar{c}_u}\right)e^{-\bar{c}_u t} \tag{41}$$

where $\bar{c}_u = -\max\{\lambda_{\max}(\boldsymbol{W}_{u11}\boldsymbol{Q}_u), \lambda_{\max}(\boldsymbol{W}_{u22}\boldsymbol{R}_u^{-1})$, and $\sigma_u\lambda_{\max}(\boldsymbol{K}_{du}) - \lambda_{\min}(\boldsymbol{K}_u)\}$, $b_u = 1/4\sigma_u\|\dot{\boldsymbol{U}}_u\|_{\infty}$.

Here, σ_u can be any appropriate positive constant and can be adjusted as needed. If matrices $\boldsymbol{W}_{u11}$, $\boldsymbol{W}_{u22}$, $\boldsymbol{Q}_u$, $\boldsymbol{R}_u^{-1}$, $\boldsymbol{K}_u$, and $\boldsymbol{K}_{du}$ are selected appropriately such that $V_u(0) - b_u/\bar{c}_u > 0$ and $\sigma_u\lambda_{\max}(\boldsymbol{K}_{du}) - \lambda_{\min}(\boldsymbol{K}_u) < 0$, and then the UUV subsystem can be ISS according to the definition given in [55].

The stability analysis of the ASV subsystem is similar to the above contents and is thus omitted here. By further taking the derivative of the overall Lyapunov candidate function V and substituting the derivative analyses of UUV and ASV into the derivative function $\dot{V}$, one can obtain that

$$\dot{V} \le -\bar{c}_u V_u - \bar{c}_a V_a + b_u + b_a \le -\bar{c}_o V + b_o \tag{42}$$

where $\bar{c}_o = \min\{\bar{c}_a, \bar{c}_u\}$ and $b_o = b_u + b_a$. According to the definition given in [55], (42) implies that the overall UUV-ASV rendezvous system is ISS. It should be noted that since the transformed ascending depth is used in the closed-loop stability analysis, the ISS property directly implies that the original collision-free rendezvous trajectory is guaranteed.

This completes the proof. ■

V. Simulation Results

In this section, simulation experiments of the UUV-ASV rendezvous scenario are conducted to demonstrate the effectiveness of the proposed method.

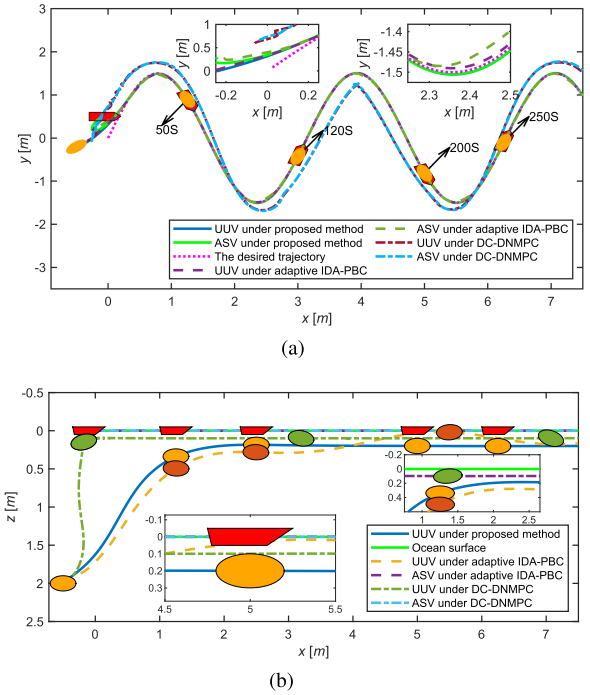

(a)

(b)

Fig. 4. Rendezvous results in different perspectives. (a) Rendezvous trajectory in the XY plane. (b) Rendezvous trajectory in the XZ plane.

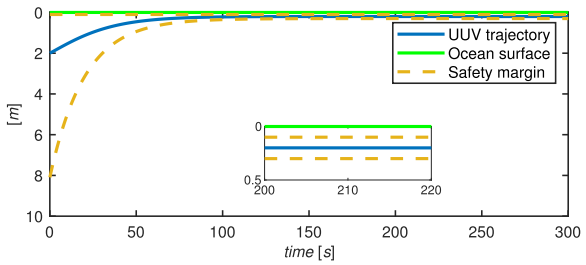

Fig. 5. Illustration of collision-free ascending for vertical rendezvous.

A. Simulation Setup

Suppose that the UUV has a parameterized predefined trajectory given as $x_{ud} = 0.025t$, $y_{ud} = 1.5\sin(0.05t)$, $\psi_{ud} = \arctan(\dot{y}_{ud}/\dot{x}_{ud})$, and $z_{ud} = 0.1$. The initial positions and velocities of two vehicles are set as $\boldsymbol{\eta}_{u0} = [-0.5, -0.2,$

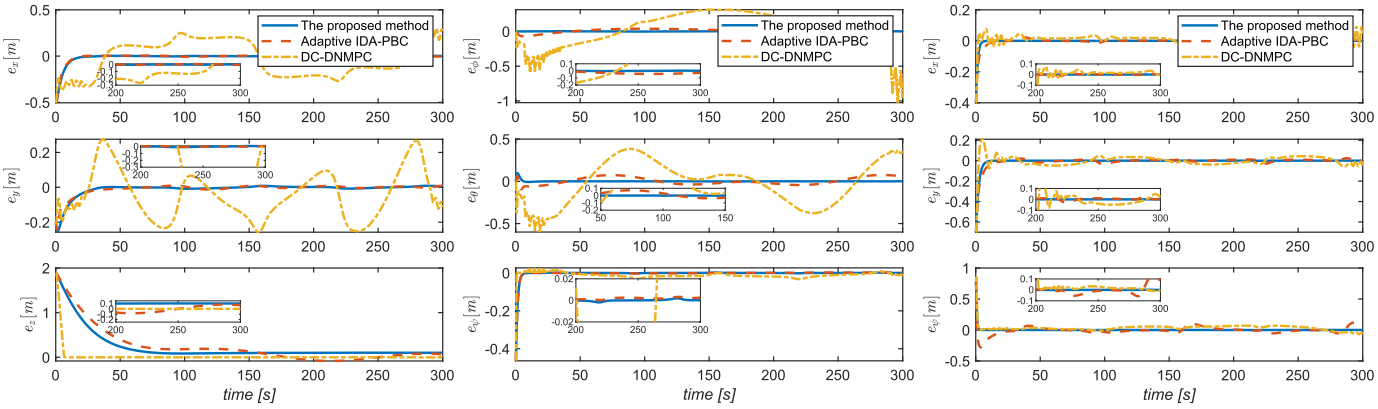

Fig. 6. Rendezvous and tracking errors. (a) Tracking errors of the UUV (position). (b) Tracking errors of the UUV (attitude). (c) Rendezvous errors between the UUV and the ASV.

$2, 0, 0, \pi/4]^\top$, $\boldsymbol{\nu}_{u0} = [0, 0, 0, 0, 0, 0]^\top$, $\boldsymbol{\eta}_{a0} = [-0.1, 0.5, 0]^\top$, and $\boldsymbol{\nu}_{a0} = [0, 0, 0]^\top$. The performance function parameters are selected as $\alpha = 0$, $\beta = 1$, $\rho_0 = 8$, $\rho_\infty = 0.2$, and $\beta_0 = 0.05$. The damping reshaping matrices are designed as $\boldsymbol{W}_{u11} = -\text{diag}([1, 1.25, 0.55, 8, 8, 7.5])$, $\boldsymbol{W}_{u22} = -\text{diag}([1, 5, 10, 5, 5, 15])$, $\boldsymbol{W}_{a11} = -\text{diag}([1, 1, 2])$, and $\boldsymbol{W}_{a22} = -\text{diag}([0.8, 0.5, 0.8])$. The gain matrices related to the lumped uncertainty observers are selected as $\boldsymbol{K}_u = \text{diag}([5, 5, 5, 5, 5, 5])$ and $\boldsymbol{K}_a = \text{diag}([10, 10, 10])$. The gain matrices for the desired Hamiltonian functions are configured as $\boldsymbol{Q}_u = \text{diag}([0.2, 0.07, 0.05, 0.05, 0.05, 0.05])$, $\boldsymbol{R}_u = \text{diag}([1, 0.8, 2, 0.2, 0.2, 0.2])$, $\boldsymbol{K}_{du} = \text{diag}([1, 1, 1, 1, 1, 1])$, $\boldsymbol{Q}_a = \text{diag}([0.8, 0.5, 2])$, $\boldsymbol{R}_a = \text{diag}([0.1, 0.1, 0.5])$, and $\boldsymbol{K}_{da} = \text{diag}([1, 1, 1])$. The nominal parts in the hydrodynamics matrices of the UUV and the ASV are set as $\boldsymbol{D}_{u0} = \text{diag}\{246.3|u_u| + 28.4, 508.8|v_u| + 37.3, 267.6|w_u|, 100.1|p_u| + 2.5, 58.4|q_u| + 4.4, 75.4|r_u| + 3\}$ and $\boldsymbol{D}_{a0} = \text{diag}\{0.5|u_a| + 6, 2.5|v_a| + 12, 0.025|r_a| + 0.25\}$. The unmodeled parts $\boldsymbol{D}_{uu}$ and $\boldsymbol{D}_{au}$ involve twelve basis matrices $\boldsymbol{D}_{uu_j}, (j = 1, \ldots, 12)$ and six basis matrices $\boldsymbol{D}_{au_k}, (k = 1, \ldots, 6)$, respectively. All of those are selected as $\boldsymbol{D}_{uu(1)} = \text{diag}([|u_u|, \boldsymbol{0}_{5\times1}])$, $\boldsymbol{D}_{uu(2)} = \text{diag}([|v_u|, \boldsymbol{0}_{5\times1}])$, $\boldsymbol{D}_{uu(3)} = \text{diag}([|w_u|, \boldsymbol{0}_{5\times1}])$, $\boldsymbol{D}_{uu(4)} = \text{diag}([|p_u|, \boldsymbol{0}_{5\times1}])$, $\boldsymbol{D}_{uu(5)} = \text{diag}([|q_u|, \boldsymbol{0}_{5\times1}])$, $\boldsymbol{D}_{uu(6)} = \text{diag}([|r_u|, \boldsymbol{0}_{5\times1}])$, $\boldsymbol{D}_{uu(7)} = \text{diag}([1, 0, 0, 0, 0, 0])$, $\boldsymbol{D}_{uu(8)} = \text{diag}([0, 1, 0, 0, 0, 0])$, $\boldsymbol{D}_{uu(9)} = \text{diag}([0, 0, 1, 0, 0, 0])$, $\boldsymbol{D}_{uu(10)} = \text{diag}([0, 0, 0, 1, 0, 0])$, $\boldsymbol{D}_{uu(11)} = \text{diag}([0, 0, 0, 0, 1, 0])$, $\boldsymbol{D}_{uu(12)} = \text{diag}([0, 0, 0, 0, 0, 1])$, $\boldsymbol{D}_{au(1)} = \text{diag}([|u_a|, 0, 0])$, $\boldsymbol{D}_{au(2)} = \text{diag}([|v_a|, 0, 0])$, $\boldsymbol{D}_{au(3)} = \text{diag}([|r_a|, 0, 0])$, $\boldsymbol{D}_{au(4)} = \text{diag}([1, 0, 0])$, $\boldsymbol{D}_{au(5)} = \text{diag}([0, 1, 0])$, and $\boldsymbol{D}_{au(6)} = \text{diag}([0, 0, 1])$. Other model parameters can be referred to Table I.

To evaluate the superiority of the proposed control method in control performance and robustness, actual disturbances induced by wind, wave, and current are considered. In practical applications, ASVs are typically subjected to coupled disturbances induced by wind and waves, whereas UUVs are primarily influenced by ocean currents. Among them, the current disturbances, with different amplitudes and periods, are relatively gentle compared with wind and wave effects. Therefore, the current disturbances are modeled in a low-frequency and bounded form as $\boldsymbol{d}_u = [-5\sin(0.06t)N, -4\sin(0.05t)N, -5\sin(0.04t) - \cos(0.02t)N, -4\cos(0.02t)N \cdot m, -2\sin(0.06t) - 3\cos(0.03t)N \cdot m, -6\sin(0.01t)N \cdot m]^\top$. In contrast, as in [46], the wind forces acting on the ASV are closely related to several factors, involving wind velocity V_{wind}, the ASV length L_a, frontal and lateral projected areas A_{F_w}, A_{L_w}, and wind angle of attack γ_{wind}. The wave-induced disturbance can be separated into two effects: zero-mean oscillatory motions called wave-frequency motion, and nonzero slowly varying components called wave drift force. Besides, the wave spectrum is simulated by a two-parameter wave spectral formulation called "Pierson-Moskowitz" (PM) spectrum system. Specific models and corresponding parameters of both wind and wave are chosen the same as those in [51]. In this article, typical sea conditions covering slight and moderate sea states (SS), that is, SS-3 with $V_{\text{wind}} = 5\ m/s$, $\gamma_{\text{wind}} = \pi/4$ rad, $A_{F_w} = 0.029\ m^2$, $A_{L_w} = 0.1255\ m^2$, $L_a = 1.225\ m$, wave height $H_{\text{wave}} = 0.54m$, and initial values of the wave drift force $\boldsymbol{d}_{\text{wave}_0} = [10\ N, 5\ N, 4N \cdot m]^\top$ are set for testing the proposed control strategy.

B. Result Analyses

Simulation results are presented in Figs. 3–6. To thoroughly demonstrate the superiority and effectiveness of the proposed approach, two representative benchmark controllers are included for comparison: the adaptive IDA-PBC controller from [41], and the disturbance-compensating distributed nonlinear MPC (DC-DNMPC) method from [24]. All controller parameters and uncertainty configurations are kept identical to ensure a fair comparison.

The rendezvous results obtained by the three methods are shown in Fig. 3. As illustrated in Fig. 3(a), the proposed method enables the ASV and the UUV to rapidly converge toward each other and achieve a coherent 3-D dynamic rendezvous. In contrast, the compared methods fail to ensure simultaneous collision avoidance and satisfactory tracking performance, as further evidenced by Fig. 4. Fig. 4(a) indicates that the ASV approaches the moving UUV efficiently,

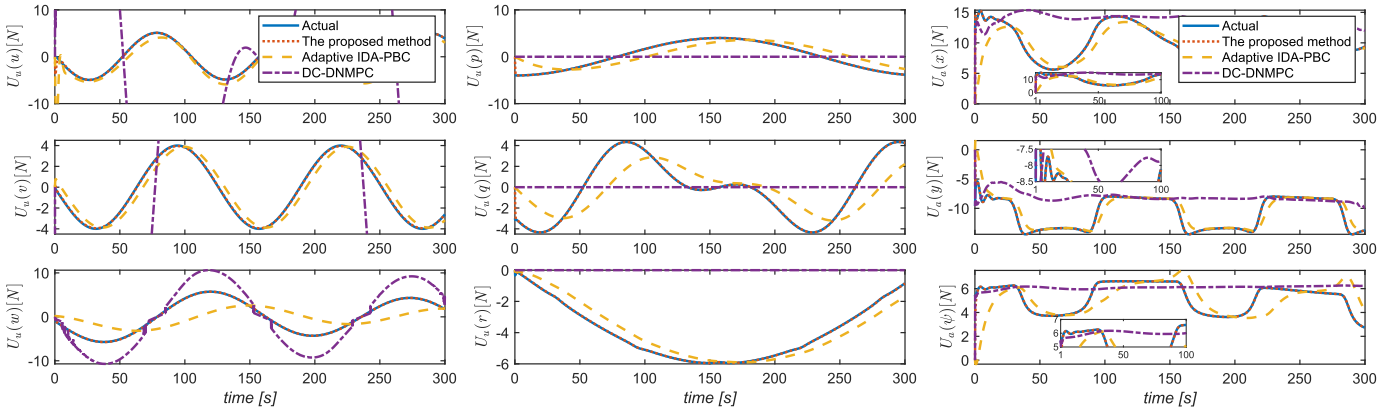

Fig. 7. Estimation results of the proposed SKUOB. (a) and (b) Estimation results for the UUV. (c) Estimation results for the ASV.

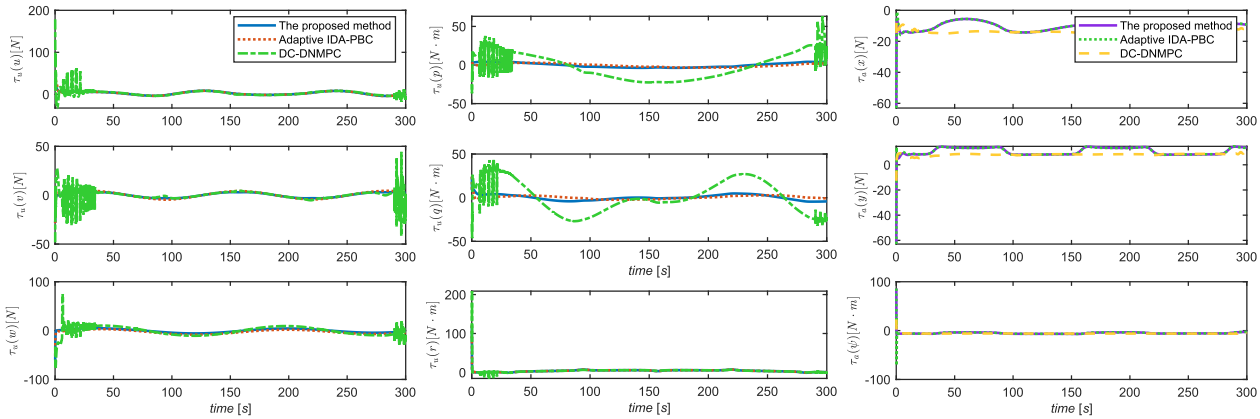

Fig. 8. Control signals of two vehicles under different methods. (a) Control inputs of the UUV (translational). (b) Control inputs of the UUV (rotational). (c) Control inputs of the ASV.

after which both vehicles maintain a quasistationary relative position throughout the rendezvous process. The ascending phase of the UUV is depicted in Fig. 4(b), showing that the proposed method produces a smooth and safe ascent trajectory. The enlarged view highlights that the proposed controller drives the UUV along a smooth constrained ascent without violating the safety-depth requirement, whereas the compared method does not meet this constraint. This observation is consistent with Fig. 5, in which the depth error remains strictly bounded within the prescribed upper and lower limits under the proposed approach. The UUV–ASV rendezvous errors and the UUV tracking errors of the predefined trajectory are summarized in Fig. 6. As shown in Fig. 6(a) and (b), the compared method exhibits much slower error convergence or even violates safety constraints, while the proposed OSK-IDA strategy achieves fast, stable, and accurate rendezvous performance, as further verified by the error curves in Fig. 6(c).

Fig. 7 plots the estimated lumped uncertainties, including SS-3-type disturbances and unmodeled dynamics, for both vehicles. The dashed curves, representing the estimates, converge accurately to the solid curves representing the true uncertainty profiles under the proposed method. In comparison, neither benchmark controller can compensate for such time-varying uncertainties. These results demonstrate that the proposed SKUOB provides reliable estimation performance under realistic environmental disturbance conditions. With accurate lumped uncertainty estimation, the resulting observer-based rendezvous control inputs for both vehicles are depicted in Fig. 8. All control signals remain within reasonable bounds, indicating that the proposed OSK-IDA approach effectively utilizes the actuator capabilities while maintaining stable and safe rendezvous behavior.

VI. Conclusion

This article presents an observer-based safety-preserving rendezvous control approach for heterogeneous marine vehicles subject to external disturbances and model uncertainties. Specifically, the interconnection and damping assignment method is used to design and analyze the control systems under the PH theory. With the proposed SKUOB algorithm, both the time-varying disturbances and unmodeled dynamics can be handled simultaneously while preserving the intrinsic interconnection structure offered by the PH framework. By incorporating the PPC technique into the IDA-PBC design method, the rendezvous safety can be ensured

despite unknown uncertainties by addressing the equivalent collision-free approaching-constrained problem under the PH framework. The overall closed-loop stability is analyzed for the UUV-ASV rendezvous system. Through comprehensive simulations, the effectiveness of the proposed OSK-IDA method is verified.

REFERENCES

[1] A. J. Sørensen, "A survey of dynamic positioning control systems," *Annu. Rev. Control*, vol. 35, no. 1, pp. 123–136, Apr. 2011.

[2] A. Veksler, T. A. Johansen, F. Borrelli, and B. Realfsen, "Dynamic positioning with model predictive control," *IEEE Trans. Control Syst. Technol.*, vol. 24, no. 4, pp. 1340–1353, Jul. 2016.

[3] E. A. Tannuri, A. C. Agostinho, H. M. Morishita, and L. Moratelli, "Dynamic positioning systems: An experimental analysis of sliding mode control," *Control Eng. Pract.*, vol. 18, no. 10, pp. 1121–1132, Oct. 2010.

[4] Y.-L. Wang, Q.-L. Han, M.-R. Fei, and C. Peng, "Network-based T–S fuzzy dynamic positioning controller design for unmanned marine vehicles," *IEEE Trans. Cybern.*, vol. 48, no. 9, pp. 2750–2763, Sep. 2018.

[5] Y. Yan, S. Yu, X. Gao, D. Wu, and T. Li, "Continuous and periodic event-triggered sliding-mode control for path following of underactuated surface vehicles," *IEEE Trans. Cybern.*, vol. 54, no. 1, pp. 449–461, Jan. 2024.

[6] L. Lapierre and D. Soetanto, "Nonlinear path-following control of an AUV," *Ocean Eng.*, vol. 34, nos. 11–12, pp. 1734–1744, Aug. 2007.

[7] M. Bibuli, G. Bruzzone, M. Caccia, and L. Lapierre, "Path-following algorithms and experiments for an unmanned surface vehicle," *J. Field Robot.*, vol. 26, no. 8, pp. 669–688, Aug. 2009.

[8] L. Lapierre and B. Jouvencel, "Robust nonlinear path-following control of an AUV," *IEEE J. Ocean. Eng.*, vol. 33, no. 2, pp. 89–102, Apr. 2008.

[9] M. Cai, Y. Wang, S. Wang, R. Wang, L. Cheng, and M. Tan, "Prediction-based seabed terrain following control for an underwater vehicle-manipulator system," *IEEE Trans. Syst., Man, Cybern., Syst.*, vol. 51, no. 8, pp. 4751–4760, Aug. 2021.

[10] N. Wang, M. J. Er, J.-C. Sun, and Y.-C. Liu, "Adaptive robust online constructive fuzzy control of a complex surface vehicle system," *IEEE Trans. Cybern.*, vol. 46, no. 7, pp. 1511–1523, Jul. 2016.

[11] Z. Jia, Z. Hu, and W. Zhang, "Adaptive output-feedback control with prescribed performance for trajectory tracking of underactuated surface vessels," *ISA Trans.*, vol. 95, pp. 18–26, Dec. 2019.

[12] H. Zheng, R. R. Negenborn, and G. Lodewijks, "Trajectory tracking of autonomous vessels using model predictive control," *IFAC Proc. Volumes*, vol. 47, no. 3, pp. 8812–8818, 2014.

[13] C. Paliotta, E. Lefeber, K. Y. Pettersen, J. Pinto, M. Costa, and J. T. de Figueiredo Borges de Sousa, "Trajectory tracking and path following for underactuated marine vehicles," *IEEE Trans. Control Syst. Technol.*, vol. 27, no. 4, pp. 1423–1437, Jul. 2019.

[14] Z. Jia, K. Zhang, Y. Shi, and W. Zhang, "Safety-preserving Lyapunovbased model predictive rendezvous control for heterogeneous marine vehicles subject to external disturbances," *IEEE Trans. Cybern.*, vol. 54, no. 9, pp. 5244–5256, Sep. 2024.

[15] J. Yan, J. Lin, X. Yang, C. Chen, and X. Guan, "Cooperation detection and tracking of underwater target via aerial–surface–underwater vehicles," *IEEE Trans. Autom. Control*, vol. 70, no. 2, pp. 1068–1083, Feb. 2025.

[16] L. Zhao and Y. Bai, "Unlocking the ocean 6G: A review of path-planning techniques for maritime data harvesting assisted by autonomous marine vehicles," *J. Mar. Sci. Eng.*, vol. 12, no. 1, p. 126, Jan. 2024.

[17] W. Hu, F. Chen, L. Xiang, and G. Chen, "Multi-ASV coordinated tracking with unknown dynamics and input underactuation via model-reference reinforcement learning control," *IEEE Trans. Cybern.*, vol. 53, no. 10, pp. 6588–6597, Oct. 2023.

[18] C. Yuan, S. Licht, and H. He, "Formation learning control of multiple autonomous underwater vehicles with heterogeneous nonlinear uncertain dynamics," *IEEE Trans. Cybern.*, vol. 48, no. 10, pp. 2920–2934, Oct. 2018.

[19] S. Dong, K. Liu, M. Liu, and G. Chen, "Cooperative time-varying formation fuzzy tracking control of multiple heterogeneous uncertain marine surface vehicles with actuator failures," *IEEE Trans. Cybern.*, vol. 54, no. 2, pp. 667–678, Feb. 2024.

[20] Y. Shi, Y. Hua, J. Yu, X. Dong, and Z. Ren, "Fully data-driven robust output formation tracking control for heterogeneous multiagent system with multiple leaders and actuator faults," *IEEE Trans. Cybern.*, vol. 54, no. 5, pp. 3183–3196, May 2024.

[21] Q. Liu, H. Yan, H. Zhang, M. Wang, and Y. Tian, "Data-driven H_∞ output consensus for heterogeneous multiagent systems under switching topology via reinforcement learning," *IEEE Trans. Cybern.*, vol. 54, no. 12, pp. 7865–7876, Dec. 2024, doi: 10.1109/TCYB.2024.3419056.

[22] D. Liu, Z. Mao, B. Jiang, and X.-G. Yan, "Prescribed performance fault-tolerant control for synchronization of heterogeneous nonlinear MASs using reinforcement learning," *IEEE Trans. Cybern.*, vol. 54, no. 9, pp. 5451–5462, Sep. 2024.

[23] M. Cai et al., "Deep reinforcement learning framework-based flow rate rejection control of soft magnetic miniature robots," *IEEE Trans. Cybern.*, vol. 53, no. 12, pp. 7699–7711, Dec. 2023.

[24] Z. Jia, H. Lu, S. Li, and W. Zhang, "Distributed dynamic rendezvous control of the AUV-USV joint system with practical disturbance compensations using model predictive control," *Ocean Eng.*, vol. 258, Aug. 2022, Art. no. 111268.

[25] H. Tang and Y. Chen, "Dynamic event-triggered distributed MPC for heterogeneous UAVs–UGVs against DoS attacks," *IEEE Trans. Aerosp. Electron. Syst.*, vol. 60, no. 6, pp. 7931–7944, Dec. 2024, doi: 10.1109/TAES.2024.3422158.

[26] Y. Zhu, S. Li, G. Guo, P. Yuan, and J. Bai, "Formation control of UAV–USV based on distributed event-triggered adaptive MPC with virtual trajectory restriction," *Ocean Eng.*, vol. 294, Feb. 2024, Art. no. 116850.

[27] H. Zhang, X. Zhang, H. Xu, and C. G. Soares, "Heterogeneous cooperative trajectory tracking control between surface and underwater unmanned vehicles," *Ocean Eng.*, vol. 301, Jun. 2024, Art. no. 117137.

[28] W. Cheng, K. Zhang, B. Jiang, and S. X. Ding, "Fixed-time faulttolerant formation control for heterogeneous multi-agent systems with parameter uncertainties and disturbances," *IEEE Trans. Circuits Syst. I, Reg. Papers*, vol. 68, no. 5, pp. 2121–2133, May 2021.

[29] W. Cheng, K. Zhang, and B. Jiang, "Fixed-time fault-tolerant formation control for a cooperative heterogeneous multiagent system with prescribed performance," *IEEE Trans. Syst., Man, Cybern., Syst.*, vol. 53, no. 1, pp. 462–474, Jan. 2023.

[30] R. Lozano, B. Brogliato, O. Egeland, and B. Maschke, "Dissipative systems analysis and control," *Theory Appl.*, vol. 2, pp. 2–5, Mar. 2000.

[31] A. van der Schaft and D. Jeltsema, "Port-Hamiltonian systems theory: An introductory overview," *Found. Trends Syst. Control*, vol. 1, nos. 2–3, pp. 173–378, Jun. 2014.

[32] R. Ortega, A. van der Schaft, B. Maschke, and G. Escobar, "Interconnection and damping assignment passivity-based control of port-controlled Hamiltonian systems," *Automatica*, vol. 38, no. 4, pp. 585–596, Apr. 2002.

[33] A. Donaire and T. Perez, "Dynamic positioning of marine craft using a port-Hamiltonian framework," *Automatica*, vol. 48, no. 5, pp. 851–856, May 2012.

[34] S. El Ferik and M. F. Emzir, "PCH-based $\mathcal{L}_2$ disturbance attenuation and control of autonomous underwater vehicle," *IFAC Proc. Volumes*, vol. 45, no. 5, pp. 192–197, 2012.

[35] L. Jin, S. Yu, Q. Zhao, G. Shi, and X. Wu, "Fixed-time H_∞ tracking control of unmanned underwater vehicles with disturbance rejection via port-Hamiltonian framework," *Ocean Eng.*, vol. 293, Feb. 2024, Art. no. 116533.

[36] H. Tanaka, H. Hirai, and K. Hosoda, "Position control of McKibben-type pneumatic artificial muscle via port-Hamiltonian approach," *IEEE Robot. Autom. Lett.*, vol. 10, no. 6, pp. 6384–6391, Jun. 2025, doi: 10.1109/LRA.2025.3567164.

[37] J. Gong, S. Guo, H. Shen, W. Wei, and Y. Long, "Path-tracking cascade control of hydraulic-tracked vehicles based on port-controlled Hamiltonian model," *IEEE Trans. Intell. Vehicles*, vol. 10, no. 1, pp. 654–667, Jan. 2025, doi: 10.1109/TIV.2024.3417213.

[38] J.-R. Montoya-Morales, M.-E. Guerrero-Sánchez, G. Valencia-Palomo, O. Hernández-González, F.-R. López-Estrada, and L. C. Félix-Herrán, "Design and experimental validation of IDA-PBC-based flight control for quadrotors," *Robotica*, vol. 43, no. 7, pp. 2376–2397, Jul. 2025.

[39] A. Donaire, J. G. Romero, and T. Perez, "Passivity-based trajectory-tracking for marine craft with disturbance rejection," *IFAC-PapersOnLine*, vol. 48, no. 16, pp. 19–24, 2015.

[40] A. Donaire, J. G. Romero, and T. Perez, "Trajectory tracking passivity-based control for marine vehicles subject to disturbances," *J. Franklin Inst.*, vol. 354, no. 5, pp. 2167–2182, Mar. 2017.

[41] Z. Jia, L. Qiao, and W. Zhang, "Adaptive tracking control of unmanned underwater vehicles with compensation for external perturbations and uncertainties using port-Hamiltonian theory," *Ocean Eng.*, vol. 209, Aug. 2020, Art. no. 107402.
[42] J. Zhao, Y. Wu, Y. Guo, Z. Li, and Y. Wu, "Distributed formation control for port-Hamiltonian multi-agent systems by average state estimation," *ISA Trans.*, vol. 164, pp. 297–309, Sep. 2025, doi: 10.1016/j.isatra.2025.05.039.
[43] C. Lv, H. Yu, J. Chen, N. Zhao, and J. Chi, "Trajectory tracking control for unmanned surface vessel with input saturation and disturbances via robust state error IDA-PBC approach," *J. Franklin Inst.*, vol. 359, no. 5, pp. 1899–1924, Mar. 2022.
[44] E. Franco, "Adaptive IDA-PBC for underactuated mechanical systems with constant disturbances," *Int. J. Adapt. Control Signal Process.*, vol. 33, no. 1, pp. 1–15, Jan. 2019.
[45] M. Ryalat and D. S. Laila, "A robust IDA-PBC approach for handling uncertainties in underactuated mechanical systems," *IEEE Trans. Autom. Control*, vol. 63, no. 10, pp. 3495–3502, Oct. 2018.
[46] T. I. Fossen, *Handbook of Marine Craft Hydrodynamics and Motion Control*. Hoboken, NJ, USA: Wiley, 2011.
[47] J.-H. Li, P.-M. Lee, B.-H. Jun, and Y.-K. Lim, "Point-to-point navigation of underactuated ships," *Automatica*, vol. 44, no. 12, pp. 3201–3205, Dec. 2008.
[48] H. Wei, C. Shen, and Y. Shi, "Distributed Lyapunov-based model predictive formation tracking control for autonomous underwater vehicles subject to disturbances," *IEEE Trans. Syst., Man, Cybern., Syst.*, vol. 51, no. 8, pp. 5198–5208, Aug. 2021.
[49] M.-C. Fang, P.-E. Chang, and J.-H. Luo, "Wave effects on ascending and descending motions of the autonomous underwater vehicle," *Ocean Eng.*, vol. 33, nos. 14–15, pp. 1972–1999, Oct. 2006.
[50] X. Ding, H. Bian, H. Ma, and R. Wang, "Ship trajectory generator under the interference of wind, current and waves," *Sensors*, vol. 22, no. 23, p. 9395, Dec. 2022.
[51] N. Wang and C. K. Ahn, "Coordinated trajectory-tracking control of a marine aerial-surface heterogeneous system," *IEEE/ASME Trans. Mechatronics*, vol. 26, no. 6, pp. 3198–3210, Dec. 2021.
[52] A. Van Der Schaft, "Port-Hamiltonian systems: An introductory survey," in *Proc. Int. Congr. Mathematicians*, 2007, pp. 1339–1365.
[53] C. Lv et al., "A hybrid coordination controller for speed and heading control of underactuated unmanned surface vehicles system," *Ocean Eng.*, vol. 176, pp. 222–230, Mar. 2019.
[54] C. P. Bechlioulis and G. A. Rovithakis, "Robust adaptive control of feedback linearizable MIMO nonlinear systems with prescribed performance," *IEEE Trans. Autom. Control*, vol. 53, no. 9, pp. 2090–2099, Oct. 2008.
[55] E. D. Sontag, "Input to state stability: Basic concepts and results," in *Proc. Nonlinear Optim. Control Theory, Lectures Given CIME Summer School Cetraro*, Jun. 2008, pp. 163–220.

Zehua Jia (Member, IEEE) received the B.Eng. degree in detection, guidance, and control techniques from Central South University, Changsha, China, in 2017, and the Ph.D. degree in control science and engineering from Shanghai Jiao Tong University, Shanghai, China, in 2023.

From 2021 to 2022, he was a Visiting Research Scholar at the Department of Mechanical Engineering, University of Victoria, Victoria, BC, Canada. He is currently a Lecturer with the School of Information and Communication Engineering, Hainan University, Haikou, China. His research interests include model predictive control, nonlinear control, and cooperative control with applications to intelligent marine systems.

Huahuan Wang (Student Member, IEEE) received the B.E. degree in electronic information engineering from Tianjing Chenjian University, Tianjing, China, in 2023. He is currently pursuing the master's degree with the School of Information and Communication Engineering, Hainan University, Haikou, China.

His research interests include nonlinear control, model predictive control, and coordinated control with applications to intelligent marine vehicle systems.

Wentao Wu (Member, IEEE) received the B.E. degree in electrical engineering and automation from Harbin University of Science and Technology, Harbin, China, in 2018, the M.E. degree in electrical engineering from Dalian Maritime University, Dalian, China, in 2021, and the Ph.D. degree in electronic information from Shanghai Jiao Tong University, Shanghai, China, in 2025.

From 2023 to 2024, he was a Visiting Research Scholar at the University of Victoria, Victoria, BC, Canada. His research interests include intelligent control, marine robotics, and cooperative autonomous systems.

Guoqing Zhang (Member, IEEE) received the B.S. and Ph.D. degrees from the Navigation College, Dalian Maritime University (DMU), Dalian, China, in 2010 and 2015, respectively.

He joined DMU as a Lecturer in 2016 and later worked as a Post-Doctoral Fellow with Shanghai Jiao Tong University, Shanghai, China. He has been a Doctoral Supervisor, since 2020, and a Professor at DMU, since 2023. His research interests include adaptive control, nonlinear control, and applications in intelligent transportation.

Dr. Zhang received the National Excellent Youth Science Fund, the National Postdoctoral Innovative Talent Award, the Ocean Engineering Technology Award (Second Class), and the National Excellent Doctoral Dissertation Award in Intelligent Transportation.

Weidong Zhang (Senior Member, IEEE) received the B.S. degree in measurement technology and instruments, the M.S. degree in applied electronic technology, and the Ph.D. degree in control theory and its application from Zhejiang University, Hangzhou, China, in 1990, 1993, and 1996, respectively.

He was a Post-Doctoral Fellow at Shanghai Jiao Tong University, Shanghai, China. In 1998, he joined Shanghai Jiao Tong University, as an Associate Professor, and since 1999, he has been a Full Professor. From 2003 to 2004, he was an Alexander von Humboldt Fellow at the University of Stuttgart, Stuttgart, Germany. In 2011, he became the Chair Professor at Shanghai Jiao Tong University. He is currently the Director of the Engineering Research Center of Marine Intelligent Systems, Ministry of Education, Shanghai, and the Engineering Research Center of Marine Automation, Shanghai Municipal Education Commission, Shanghai. He has authored more than 300 refereed papers and a book, and holds more than 100 patents. His research interests include control theories and their applications in several fields, including industrial processes and intelligent unmanned systems.

Prof. Zhang was a recipient of the National Science Fund for Distinguished Young Scholars of China and Shanghai Subject Chief Scientist.